

# An electrochemically actuated drug delivery device with *in-situ* dosage sensing

Ying Yi<sup>1</sup> , Mu Chiao<sup>2</sup> and Bo Wang<sup>1,\*</sup> 

<sup>1</sup> Division of Information and Computing Technology, College of Science and Engineering, Hamad Bin Khalifa University, Doha, Qatar

<sup>2</sup> Department of Mechanical Engineering, University of British Columbia, Vancouver, Canada

E-mail: [bwang@hbku.edu.qa](mailto:bwang@hbku.edu.qa)

Received 10 October 2020, revised 21 January 2021

Accepted for publication 12 March 2021

Published 24 March 2021



## Abstract

Very few conventional micro-electro-mechanical systems as drug delivery devices have *in-situ* dosage monitoring sensors, this thus brings inaccurate released dose, which results in either inefficient pharmaceutical effects or over-dose induced side effects. In this work, we integrate a low-cost piezoresistive sensor with an electrochemically actuated drug delivery device, and investigate its dosage monitoring performance. Different from the conventional sensor fabrication based on mixing conductive particles into liquid polymer, our proposed sensor is constructed from solidified carbon ink film embedded in a polydimethylsiloxane (PDMS) membrane, which can obtain an optimum tradeoff between the gauge factor and maximum achievable displacement. An electrolytic reaction induces the electrolysis-bubble in the actuator chamber with an increase in pressure, which causes displacement of the PDMS sealing membrane. This provides the actuation force to deliver the drug solution. The displacement of the PDMS membrane that determines the pumped volume of the drug solution is quantified through a resistance change of the embedded piezoresistive sensor. We report a single pumping volume of up to 7  $\mu\text{l}$ , which is monitored by the resistance change ratio ( $\Delta R/R$ ), ranging from 2% to 12% with a dosage sensing accuracy of  $\pm 6.5\%$ .

Supplementary material for this article is available [online](#)

Keywords: solidified carbon ink, drug delivery device, dosage monitoring

(Some figures may appear in color only in the online journal)

## 1. Introduction

Implantable drug delivery devices are gaining popularity for use in various therapies [1], such as treatment for brain tumors [2], prostate cancer [3], and anabolic osteoporosis [4]. As an important part of drug therapy, the drug concentration must be maintained within an effective therapeutic window [5], to reduce side-effects. Some potent drugs require a precise dosage, for example,  $\sim 300 \mu\text{g}$  of epinephrine

is required to treat anaphylactic shock [6]. Moreover, the flow rate of drug delivery devices must be consistent or less than the flow rate of bodily fluids to reduce risks of drug overdose to non-targeted cells. For example, the preferred flow rate of ocular drug delivery should be less than  $2 \mu\text{l min}^{-1}$  [7], because the ciliary body of the eye produces aqueous humor at a rate of  $2.4 \pm 0.6 \mu\text{l min}^{-1}$  in adults [8]. Micro-fabricated, controlled release drug delivery devices have addressed the dimensional requirements of implants [9, 10]; however, devices with integrated sensors that monitor the actual dosage and flow rate have rarely been explored [11]. Previously, micro-electro-mechanical systems, based on an

\* Author to whom any correspondence should be addressed.

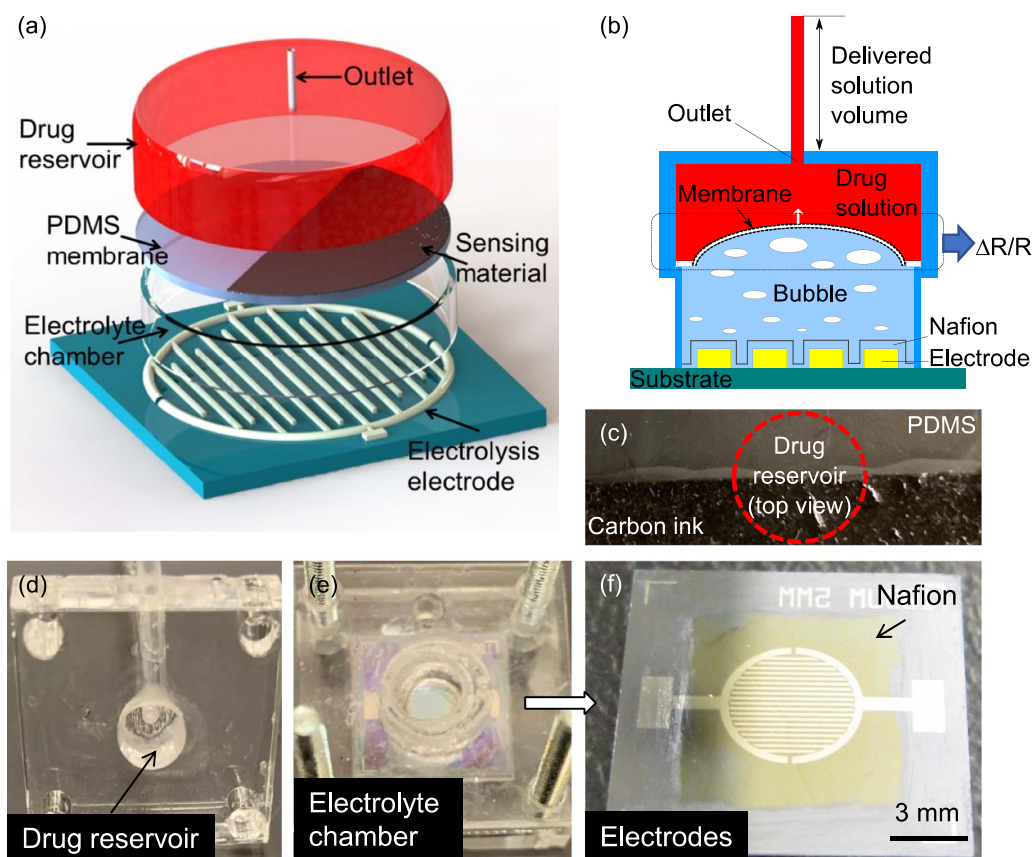


**Figure 1.** (a) Schematic exploded view of the pump showing major components; (b) cross-sectional view of the assembled pump showing working principle; (c) the prototype of the thin PDMS membrane embedded with a conductive carbon ink layer and the actual functioning part of the sensor; (d) the drug reservoir was simply fabricated from a PMMA board; (e) the assembled electrolytic actuator with a PMMA sheet to hold the PDMS membrane; (f) layout of Nafion-coated Pt/Ti electrodes.

electrolytic actuator, was shown to deliver drug solutions [5, 12]. Electrolytic mechanisms show significant advantages in terms of low power consumption, high flow rate (up to  $\sim 142 \mu\text{l min}^{-1}$  [13]), and stability [14], when compared to other actuations using magnetic [15, 16], electrostatic [17], piezoelectric [18], electromagnetic [19], or osmotic [20] mechanisms.

In this paper, we report a new electrolytic drug delivery device with an integrated dosage sensor. As shown in figure 1, deformation of an elastic polydimethylsiloxane (PDMS) membrane caused by an electrolysis-bubble induced pressure increase inside the electrolytic chamber, which provides drug delivery actuation [5, 21]. The pumped volume of the drug solution can be directly quantified via the degree of membrane deformation. An ultra-thin sensing film is embedded in the membrane, providing a signal output that corresponds to the membrane deformation while driving the drug solution. The transduction of the pressure sensor in response to an external force (or mechanical strain) involves a piezoelectric [22, 23], capacitive [24, 25], or piezoresistive [26–28] mechanism. These transduction mechanisms have their own merits, while the selection of a particular sensing approach mainly depends on the target application [29–31]. For the purpose of diaphragm actuating the drug solution, the membrane must be sufficiently elastic so that it can provide

a large achievable displacement under the electrolysis-bubble pressure. Piezoelectric sensors that use a stiff piezoelectric material layer [32] or that only work in dynamic tension conditions [33] are not suitable. Capacitive sensors are made of two parallel conductive electrodes and a compliant dielectric layer that is placed between the two electrodes. Obviously, this kind of sensor may not be sensitive to the displacement of the diaphragm as the stretching over the surface of the elastic membrane would dominate over the compression in the dielectric layer.

A piezoresistive sensor has a simple design structure and read-out approach [34]. It can provide high pressure sensitivity and quick responses [35], all of which are desired features for the dosage sensing in the new drug delivery device. Unfortunately, piezoresistive materials are usually stiff, which can reduce the flexibility and elasticity of the final membrane after it is integrated with the piezoresistive sensor. Considering that diaphragms must be stretchable to meet the desired volume of drug delivery while maintaining high sensitivity to strain, a flexible piezoresistive pressure sensor would be necessary for this new device. Differing from the conventional approach of dispersing conductive particles into liquid polymer (i.e. the carbon black (CB)-PDMS composite [36]), we directly immerse solidified carbon ink film [37], comprised of CB nano-particles in

tight contact [38] into liquid PDMS. The solidified carbon ink film is ‘paper like’, ultra-flexible, and piezoresistive. It provides a highly sensitive resistance change ratio ( $\Delta R/R$ ) corresponding to the displacement of the PDMS membrane because the tension can lead to changes in the geometric shape of the sensing film, and enlarged gaps between conductive CB particles, thus resulting in an increasing tendency of the resistance according to tunneling effects theory [39]. A preliminary proof of concept for the electrochemically actuated drug delivery device using a piezoresistive sensor prototype is presented here, and its capability for tracking the delivered volume is emphasized. The flow rate can be obtained by dividing the pumped volume by the time spent pumping. Our proposed dosage and flow rate sensing is straightforward and accurate technique would be appropriate for future drug delivery devices with active control and real-time monitoring future drug delivery devices with active control and real-time monitoring.

## 2. Design and fabrication

### 2.1. Design of the drug delivery device

Figure 1(a) illustrates the design of our proposed drug delivery device, with its assembled structure shown in figure 1(b). Components including the sensor (figure 1(c)), drug reservoir (figure 1(d)), and electrolyte chamber (figure 1(e)) were not permanently bonded together to reduce the device’s size, but they were assembled by tightening polymethyl methacrylate (PMMA) holders for the purpose of testing. A rectangular solidified carbon ink layer (15  $\mu\text{m}$  in thickness, 3.5 mm in width, and 2.6 cm in length) was embedded into a PDMS membrane (130  $\mu\text{m}$  in thickness, 8 mm in width, and 2.2 cm in length). The two ends of the carbon ink layer beyond the PDMS membrane were fabricated as contact pads. The PDMS membrane was placed between the electrolyte chamber and the reservoir, to avoid contaminating the electrolyte and the electrochemical interaction with the drug solution. Only the deformable part of the membrane that covered the bottom of the drug reservoir was regarded as the actual functional area of the piezoresistive pressure sensor (figure 1(c), to be explained in the following subsections).

The drug reservoir was drilled in a 6 mm thick PMMA board (Moden Glas Acrylic Co., Ltd) using a  $\text{CO}_2$  laser cutter (Universal PLS6.75); its dimensions were 2.4 mm in radius and 4 mm in depth. The electrolyte chamber was fabricated by gluing a PMMA loop onto the electrolysis-electrode base (figure 1(f)). The dimensions of the loop included an inner radius of 2.5 mm and height of 2.7 mm. A thin PMMA sheet (1 mm) including a hole with the same radius as the loop was directly glued on the top of the chamber to support the soft PDMS membrane. The electrode was fabricated by sputtering titanium/platinum (Ti/Pt) on a silicon wafer, having an interdigitated layout with radius of 2.5 mm and height of 300 nm. The electrode was coated with a Nafion film of 220 nm to improve the electrolysis efficiency. The detailed fabrication process and dimensions of the electrode were demonstrated [40].

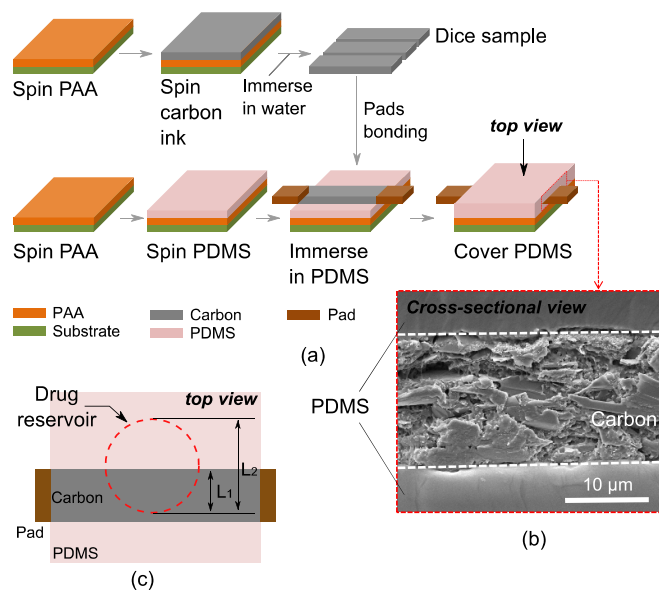


**Figure 2.** (a) Flow diagram of the sensor membrane fabrication procedure; (b) the cross-sectional view of the PDMS membrane embedding the solidified carbon ink layer; (c) illustration of the functional part of the sensor membrane.

### 2.2. Fabrication of the sensor membrane

The integration of the carbon ink film with the PDMS membrane that uses resistance change as a sensing parameter to characterize the pumped volume of drug solution is the focus of this work. Figure 2(a) illustrates the fabrication process of an ultra-thin carbon ink film embedded between two PDMS layers. The first process step was to prepare the solidified carbon ink film. Its fabrication began by preparing a polyacrylic acid (PAA) solution and the carbon ink. The PAA solution was synthesized by dissolving PAA powder ( $M_w = 1800$ , Sigma-Aldrich) in distilled water at a 25% w/v concentration and it was then filtered through a sterile 0.45  $\mu\text{m}$  PVDF syringe filter (Millipore Corporation, USA). The carbon ink used in this work was made by mixing CB nano-particles with ethylene glycol (~18 wt.%), with a viscosity of about ~22 cP [38]. The PAA solution was spun onto glass substrates at 500 rpm for 10 s and then at 800 rpm for 30 s. The glass slides were then baked at 150  $^{\circ}\text{C}$  on a hotplate for 5 min. The dried PAA coating was used as a sacrificial layer for the following carbon ink film and PDMS membrane. The carbon ink was then spun-coated on the glass slide (20 s at 500 rpm, 1 min at 1500 rpm) and then dried at 120  $^{\circ}\text{C}$  for 5 min. The solidified carbon ink layer was peeled off from the glass slide after immersing it into water for 3 h, and tailored into a rectangular shape. Finally, conductive copper tapes were bonded to the ends of the rectangular carbon ink film, as contact pads for resistance measurements.

The second process step was an integration of the above-processed carbon ink film with the PDMS membrane. Liquid PDMS was spun onto the other PAA-coated glass substrate (20 s at 400 rpm, 1 min at 1500 rpm), and followed by placing the carbon ink film on the top of the PDMS. The new PDMS was then poured to cover the entire carbon film and spun again (3 min at 400 rpm) to form a uniform membrane

surface. After a drying process (150 °C, 5 min) and immersing the sensor membrane in water for 5 h, the PDMS membrane was cured and peeled off the glass substrate, showing a ‘sandwich’ structure of carbon ink film embedded in two PDMS layers. The corresponding SEM image is shown in figure 2(b). The porous structure of the inner solidified carbon ink film is formed when the solvent in the carbon ink evaporates during the drying process. The fabricated sensor membrane was deployed in between the PMMA holder of the electrolytic chamber and the drug reservoir, the red round ring (schematically illustrated in figure 2(c)). It shows the functional sensor area that was sealed by the drug reservoir and electrolytic chamber, as well as the corresponding carbon coverage ratio. The whole PDMS membrane was not covered by carbon ink film in consideration of the elasticity (or the achievable deformation) of the sensor device. Following the fabrication procedure, a batch of five sensor samples were produced and tested under different levels of strain.

### 3. Experimental analysis and results

#### 3.1. Sensor characterization

The stress–strain curves of all PDMS membranes with embedded carbon ink layers with different coverage ratios (25%, 50%, 75%, and 100%) were measured using a dynamic mechanical analyzer (DMA Q8000, PerkinElmer Inc., Waltham, MA, USA). The tested samples were tailored into a rectangular shape with 15 mm in length, and 10 mm in width to meet the physical testing requirements of the DMA. The two ends of the sample were clamped and stretched with a ramp force of 4.5 N min<sup>-1</sup> to achieve up to a 8.5% strain. After testing in air, the sample was kept clamped and switched to immersion mode in a water bath. The same DMA setup was also executed for the pure PDMS sample with the same dimensions as those in the control experiments. A digital multimeter (Keithley 2110, Tektronix, Beaverton, OR, USA) that was electrically connected to the two conductive pads of the sensor was used to record the sensor’s output resistance.

Figure S1 (available online at [stacks.iop.org/SMS/30/055003/mmedia](https://stacks.iop.org/SMS/30/055003/mmedia)) demonstrates the elasticity of the PDMS membrane embedded with different coverage ratios of carbon ink layer, as well as the  $\Delta R/R$  as a function of strain (denoted as ‘ $\epsilon$ ’). The coverage ratio of the carbon ink from 25% to 100% corresponds to an increasing gauge factor from 1.9 to 21.1. Obviously, for the same weight of sensing material, the sensor that was fabricated using the above-mentioned procedure provides a higher gauge factor than ones that mix CB into liquid PDMS [36]. Although the PDMS membrane with higher coverage ratio of carbon ink provides higher sensitivity to strain, its mechanical elasticity is reduced accordingly. The sensor device with a carbon coverage ratio of 50% ( $L1/L2$  as shown in figure 2(c)) was selected as a compromise between mechanical elasticity and sensitivity. The measured  $\Delta R/R$  as a function of strain is shown in figure 3. The sensor has a linear relationship with the strain up to 8.5%, beyond which the carbon layer would break. Within the safe strain range, a mean  $\Delta R/R$  of 4.4%–33.25% was achieved for a strain from

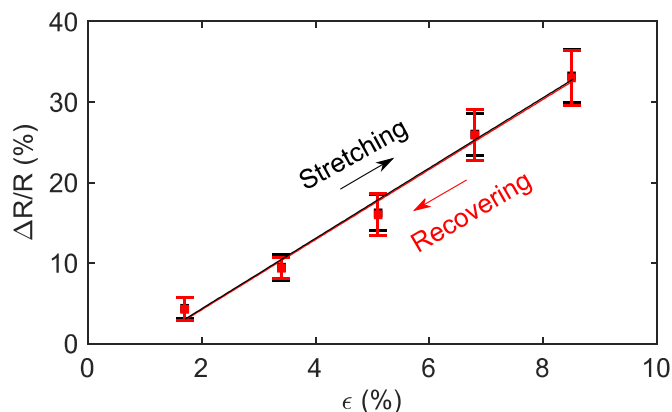


**Figure 3.** The  $\Delta R/R$  of batch-fabricated sensors at different levels of strain.

1.7% to 8.5%, respectively. Once the tension was removed, the sensor exhibited an excellent recovering ability (<1% of error). The slight  $\Delta R/R$  difference of the sensor under stretching and recovering indicates that the sensor behaves elastically within the safe strain limit.

To test the stability, recovering time, and repeatability of the sensor, figures 4(a) and (b) show the  $\Delta R/R$  of the sensor at different levels of tensions and its stability under static strain. The sensor outputs were measured with a strain starting from 0% and progressing to 8.5% in steps of 1.7%, with 8 s for each transition followed by 22 s of holding. During the holding time, the resistance of the sensor was maintained at a stable level (figure 4(a) inset). To further verify the repeatability of the sensor and reliability of the proposed fabrication approach, a repeated ‘stretching and releasing’ test was performed. The DMA was used to repeatedly stretch and recover the proposed sensor device 300 times, with each cycle being 30 s. The PDMS membrane was stretched to a maximum strain of 5.1%, and then released to its original state. Figure 4(c) shows the resistance change of the sensor for 300 cycles, with each cycle of 15 s for stretching and another 15 s for releasing. No significant resistance shift was observed in the operation cycle, this result implies that the sensor can maintain excellent repeatability as long as it is stretched within a safe limit. Zooming in the measurement data shows six mechanical cycles and the corresponding  $\Delta R/R$  (figure 4(d)). The resistance output of the sensor increased to the peak and dropped to its base level corresponding to the sensor being stretched to the maximum strain and then released to the un-tensile level. Overall, the peak  $\Delta R/R$  at a strain of 5.1% was maintained at an average level of about 17.2% over the cyclic operations.

#### 3.2. Displacement measurements of the sensor

Figure 5(a) shows the measurement setup to demonstrate the characterizations of the sensor. The measurement setup was composed of a laser Doppler vibrometer (LDV) (OFV-5000, Polytec Inc., Irvine, CA, USA), an oscilloscope (Tektronix UK Limited, Bracknell, UK), a DC power source (E3631A, Keysight Technologies, Santa Rosa, CA, USA), and a digital multimeter. The LDV was used to make non-contact displacement

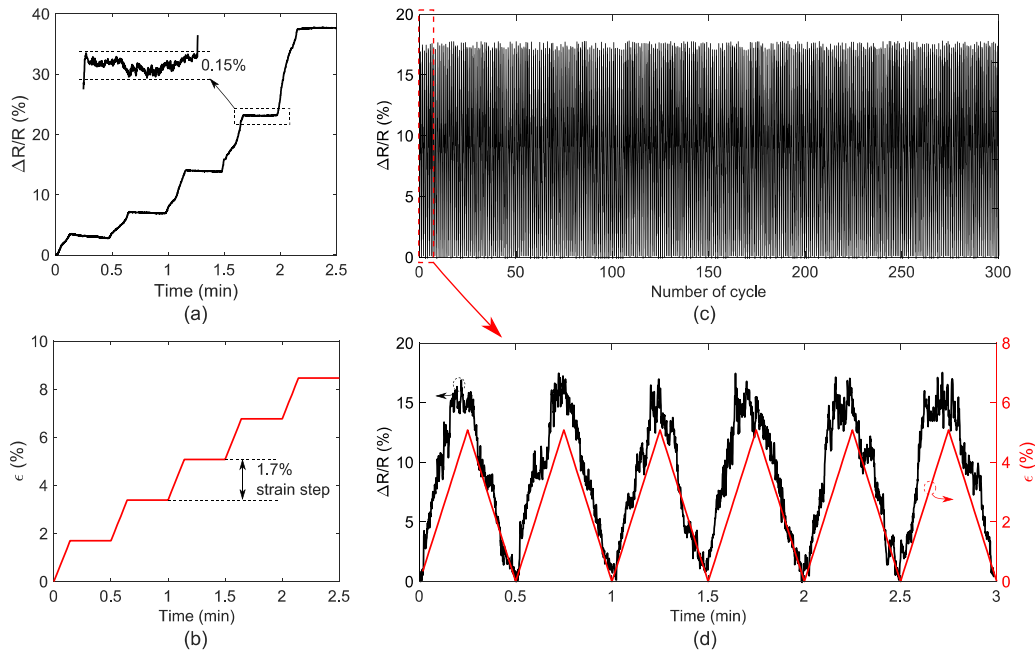


**Figure 4.** (a) The  $\Delta R/R$  measurement of the sensor under increasing strain and followed by a static tension condition; (b) the corresponding strain as a function of time; (c) the  $\Delta R/R$  of the sensor under 300 cycles of stretching and releasing operations of the PDMS membrane; and (d) magnified image of the first six cycles of the operations.

measurements of the PDMS membrane. When DC power was applied to the electrolysis-electrode, the Deionized water (DI) water in the electrolyte chamber is electrolyzed into hydrogen ( $H_2$ ) and oxygen ( $O_2$ ). Consequently, the pressure inside the chamber increases. The PDMS membrane was tightly clamped between two PMMA holders, and only the part of the membrane that covered the top of the chamber was deformed during the electrolysis-bubble expansion, which acted as the dosage sensor. This displacement of the membrane determines the delivered drug volume. The digital multimeter that electrically connects with the pads of the sensor can measure the resistance change as a function of the membrane displacement.

The displacement and the  $\Delta R/R$  of the sensor membrane were measured at different levels of power applied to the electrolytic actuator electrodes. As shown in figure 5(b), the maximum membrane displacements using a power of 2.5 mW, and 5 mW were 0.96 mm and 1.62 mm within 30 s, respectively. Apparently, higher power applied to the electrolysis-electrode causes a faster electrolysis-bubble generation rate, which in turn, results in faster membrane deformation. Moreover, when 5 mW was applied, the displacement reached the peak in about 28 s, while no significant displacement change was observed in the following 2 s of ‘power on’. This implies that 1.62 mm is the displacement limit of the designed sensor membrane. The upward displacement provides the actuation force to deliver the drug solution, but after turning off the power, the membrane slowly reverts towards its flat state, reflected by a downward trend of displacement. This occurs because the electrolysis-bubbles ( $O_2$  and  $H_2$ ) are recombined into water in the presence of the Pt electrode that has the catalytic property of reversing the electrolytic reaction [5]. Note that the step-shaped decreasing curve is mainly caused

by the limited resolution of the LDV, rather than the non-continuous bubble recombination. The expansion and restoration of the membrane are precisely presented by the sensor’s signal output. The peak  $\Delta R/R$  were 2.1% and 9.3% for cases that applied powers of 2.5 mW and 5 mW, respectively. As can be seen,  $\Delta R/R$  linearly increased with the time when a power of 2.5 mW was applied, this resistance change is caused by the changes in the geometric shape of the sensing film and enlarged gaps between conductive CB particles. When a high power was applied (e.g. 5 mW),  $\Delta R/R$  sharply increased with time because electrolysis-bubble generation rate would be high to cause cracks in the carbon ink layer due to the stretchable nature of the substrate under high tension in an ultra-short period, the principle of the resistance change is mainly depending on the disconnection and reconnection of the crack fractures in the conductive links [37]. Moreover, a noise test was implemented to clarify the measurement noise, as demonstrated by figure S2.

It is challenging to obtain the actual pressure change inside the electrolytic chamber and the resulted deformation shape of the membrane, therefore, a simulation was implemented to demonstrate the displacement of the membrane as a function of the pressure. A pressure range of 4–215 KPa was chosen for the simulation. As illustrated in figure 5(c), the shape of the membrane was demonstrated by a finite element analysis performed using COMSOL Multiphysics. An irregular dome-shape of the membrane under the applied pressure can be seen because Young’s modulus of the pure PDMS membrane part is much smaller than that of the solidified carbon ink film embedded area (as shown in figure S1(a)), resulting in different deformation levels in these two areas. It can be seen that the carbon ink is stretched in accordance with

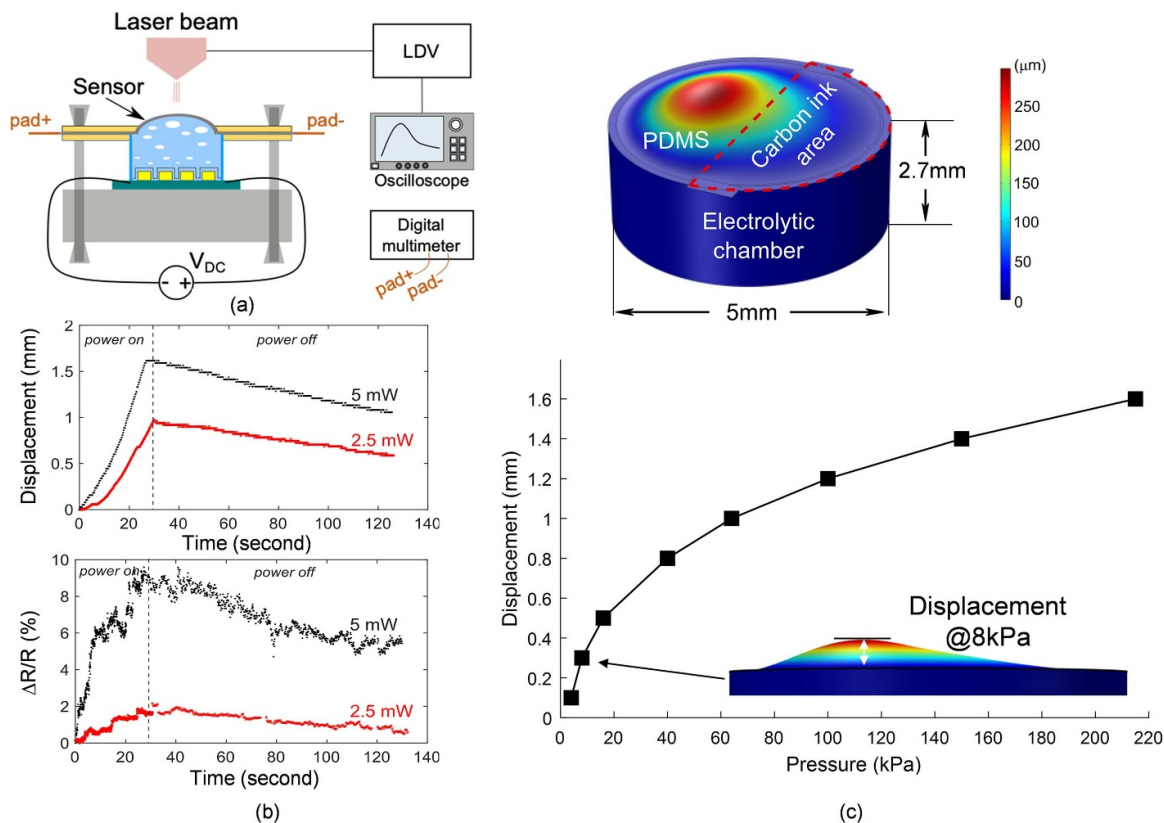


**Figure 5.** (a) Schematic diagram of the experimental setup to characterize the displacement of the membrane (without drug reservoir) and sensing performance; (b) displacements of the sensor membrane caused by the electrolysis-bubble with different input powers and the corresponding  $\Delta R/R$  under the same conditions; (c) simulation results of the sensor membrane shows the shape of the membrane under a pressure of 8 KPa and the displacement of the membrane under different pressures.

the deformation of the PDMS membrane. The displacement is defined as the largest vertical distance between the flat and the deflected membrane surface. Figure 5(c) shows that displacement of the PDMS membrane logarithmically increased from 0.1 mm to 1.6 mm within the chosen pressure range. The simulation result can estimate that the electrolysis-induced pressure was about 215 KPa for reaching the displacement peak.

### 3.3. Sensing performance in drug delivery

The complete drug delivery device assembly, with the electrolytic chamber, the drug reservoir, and the *in-situ* dosage sensor was operated to investigate the pumped volume and the corresponding  $\Delta R/R$ . Figure 6(a) shows the drug delivery device prototype. A red food coloring dye that substituted for the drug solution was injected through the inlet before it was clamped. When the electrolysis-bubble expansion caused the sensor membrane to be deformed, the dye flowed along a capillary tube at the outlet of the device. Such a moving volume can be regarded as the pumped volume. Figure 6(b) shows the drug flow rate at different levels of applied power. Increasing the power from 1.25 mW to 10 mW resulted in an increase in average flow rate from  $4.37 \mu\text{l min}^{-1}$  to  $19.75 \mu\text{l min}^{-1}$ . As shown in figure 6(c), within the safe displacement limit of the membrane, the  $\Delta R/R$  increased from 2% to 12%, corresponding to a logarithmical increase of the

pumped volume from  $0.8 \mu\text{l}$  to  $7 \mu\text{l}$ , beyond which the  $\Delta R/R$  exhibited a sharp increase trend for the volume increase. This implied that a volume of  $7 \mu\text{l}$  was close to the maximum achievable displacement of the PDMS sealing membrane. In other words, the delivered drug volume can be estimated using the sensor output  $\Delta R/R$  and a governing fitting curve within a volume range of up to  $7 \mu\text{l}$ . The dosage sensing accuracy was thus  $\pm 6.5\%$ .

Take an example of the  $\Delta R/R$  tracking the volume. When a power of 4 mW was applied to the electrolysis-electrode for 30 s and then removed (figure 6(d)), the pumped drug volume steadily increased to  $5.1 \mu\text{l}$  with  $\Delta R/R$  closely tracking the change. Eventually, it reaches its peak value of 7.4% before the power is off. It can be observed that the  $\Delta R/R$  increased linearly with the volume because the cause of the resistance change kept the same before the membrane achieved its ‘over-stretched’ level (defined as a level that cracks occur [27]). This point can be backed by the linear increase of pumped volume- $\Delta R/R$  within the volume range up to about  $5.5 \mu\text{l}$ , beyond which the  $\Delta R/R$  increased exponentially for the volume increase, as shown in figure 6(c). As previously mentioned, once the power was removed, the recombination of the electrolysis-bubble restored of the PDMS membrane, which was reflected by the dye flowing through the capillary in the reverse direction. The sensor can also provide consistent  $\Delta R/R$  with the restoration of the PDMS membrane.

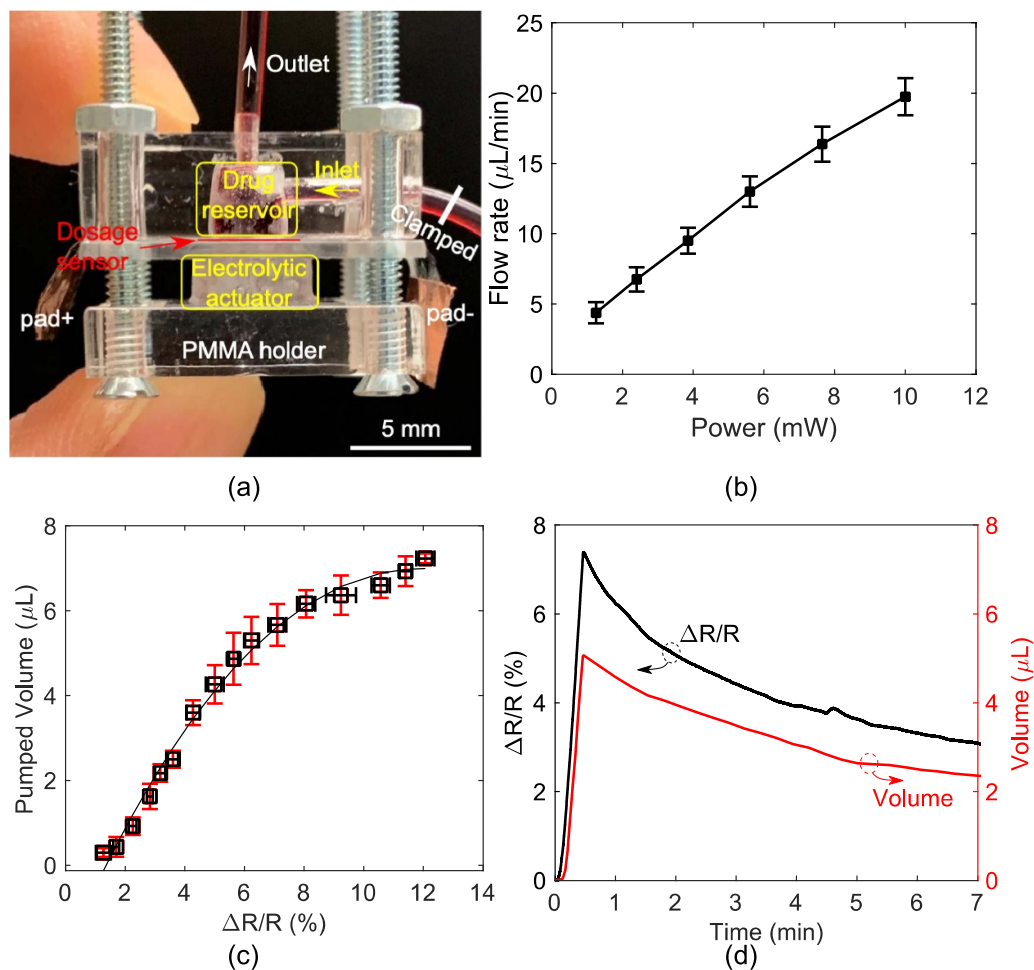


**Figure 6.** (a) The assembled drug delivery device prototype for dosage monitoring; (b) flow rates of the electrolytic pump using the proposed sensor membrane under different levels of input power; (c) experimental measurements show the relationship between the  $\Delta R/R$  and the pumped volume in electrolytic reactions; (d) volume profile of the drug delivery device with an applied power of 4 mW and the corresponding  $\Delta R/R$  of the sensor for the volume change.

#### 4. Discussion

As an emphasized point of this work, our proposed sensing approach is not only suitable for a diaphragm-driven device that delivers a liquid drug with a well-defined concentration, but it can also be used as a reciprocating-actuation-based drug delivery device [12, 41]. For example, devices using a solid drug in the reservoir (SDR) approach require a reverse flow from outside the device to dissolve the remaining solid-state drug in the reservoir. The volume drop, as shown in figure 6(d) can be regarded as a refilling volume, which is a desirable feature in an SDR device. In general, the refilled liquid of the SDR device dissolves the solid-state drug and forms a new saturated solution during the non-actuation period. The purpose is to avoid an unpredictable dosage issue. Therefore, both the released and refilled volumes must be monitored. Clearly, the  $\Delta R/R$  profile was being tracked with the volume being pumped by the bubble generation and refilling volume due to the bubble recombination in this work. Future work along this paper will involve further refinement of the sensor design and system constructions including the following:

First, even though the elastic module of the PDMS dramatically decreases with an increasing thickness [42], and an ultra-thin film may be easily broken with the expansion of the electrolysis-bubble, the compromise between robustness and elasticity must be carefully considered. Second, compared to existing electrochemical dosing sensors (with an accuracy of  $\pm 10\%$ – $15\%$  [11]), this piezoresistive sensor is more accurate and the corresponding sensing mechanism is more straightforward. In any case, a more stretchable and sensitive membrane sensor would be needed to fit the demand for dosage monitoring. Different patterns of the sensing layers, such as symmetric patterns, may be needed further to optimize the device performance. Third, although gas permeability of PDMS is a potential issue for a long-term application, this issue does not affect the sensing and actuation performance, and it does not cause detectable gas leakage within a short experimental time. A proper biocompatible and gas-sealing coating layer, such as Parylene C is required to prevent gas leakage in future work. Fourth, even though the resistance shift of the sensor caused by the temperature change was not observed due to the limited electrolytic reaction time ( $< 1$  min) and undetectable

heat transfer from the electrolyte to the sensor, the resistance sensitivity to the potential temperature change should be considered. For the purpose of obtaining accurate readings, calibration techniques may be required. Finally, the integration of the telemetry circuit to achieve the digital signal transmission between the implant and an external reader device is our final target. A highly effective resonance-based wireless power transfer technique [43, 44] can be used to provide the required power.

## 5. Conclusion

A flexible piezoresistive sensor that has a carbon film embedded into a thin PDMS membrane was designed and characterized. In our current design (e.g. carbon ink coverage ratio of 50%), the sensor provides a linear resistance change with strain. A mean  $\Delta R/R$  of 33.25% was achieved at a strain of 8.5%. The sensor also maintains a stable resistance output under static tension, exhibiting durable sensing performance. Under a low level of strain (e.g. 5.1%), the  $\Delta R/R$  of the sensor maintained exactly the same track as the change in tension on the membrane. The sensor was deployed between the electrolytic chamber and the drug reservoir to drive the drug solution when the electrolysis-bubble induced membrane displacement. The sensor can output a  $\Delta R/R$  that corresponds with the degree of membrane deformation, thereby indicating the volume of the drug being delivered. For a sensor prototype with the current sensing mechanism, the  $\Delta R/R$  increased from 2% to 12%, reflecting a polynomial increase in the volume from 0.8  $\mu\text{l}$  to 7  $\mu\text{l}$ , with a high quantification accuracy of  $\pm 6.5\%$ . In the device's actual application, the volume can be estimated by fitting a curve to the experimental data.

## ORCID iDs

Ying Yi  <https://orcid.org/0000-0003-1692-6118>

Bo Wang  <https://orcid.org/0000-0002-9359-4869>

## References

- [1] Talebian S, Foroughi J, Wade S J, Vine K L, Dolatshahi-Pirouz A, Mehrali M, Conde J and Wallace G G 2018 Biopolymers for antitumor implantable drug delivery systems: recent advances and future outlook *Adv. Mater.* **30** 1706665
- [2] Lee J, Cho H R, Cha G D, Seo H, Lee S, Park C K and Kang T 2019 Flexible, sticky, and biodegradable wireless device for drug delivery to brain tumors *Nat. Commun.* **10** 1–9
- [3] Struss W J et al 2017 Magnetically-actuated drug delivery device (MADDD) for minimally invasive treatment of prostate cancer: an *in vivo* animal pilot study *Prostate* **77** 1356–65
- [4] Farra R, Sheppard N F, McCabe L, Neer R M, Anderson J M, Santini J T, Cima M J and Langer R 2012 First-in-human testing of a wirelessly controlled drug delivery microchip *Sci. Transl. Med.* **4** 122ra21
- [5] Yi Y, Buttner U and Foulds I G 2015 A cyclically actuated electrolytic drug delivery device *Lab Chip* **15** 3540–8
- [6] Lavan D A, McGuire T and Langer R 2003 Small-scale systems for *in vivo* drug delivery *Nat. Biotechnol.* **21** 1184–91
- [7] Li P Y, Shih J, Lo R, Saati S, Agrawal R, Humayun M S, Tai Y C and Meng E 2008 An electrochemical intraocular drug delivery device *Sensors Actuators A* **143** 41–8
- [8] Ethier C R, Johnson M and Ruberti J 2004 Ocular biomechanics and biotransport *Annu. Rev. Biomed. Eng.* **6** 249–73
- [9] Zhang H, Jackson J K and Chiao M 2017 Microfabricated drug delivery devices: design, fabrication, and applications *Adv. Funct. Mater.* **27** 1703606
- [10] Cobo A, Sheybani R and Meng E 2015 MEMS: enabled drug delivery systems *Adv. Healthcare Mater.* **4** 969–82
- [11] Sheybani R, Cobo A and Meng E 2015 Wireless programmable electrochemical drug delivery micropump with fully integrated electrochemical dosing sensors *Biomed. Microdevices* **17** 74
- [12] Yi Y and Kosel J 2017 A remotely operated drug delivery system with dose control *Sensors Actuators A* **261** 177–83
- [13] Sheybani R and Meng E 2012 High-efficiency MEMS electrochemical actuators and electrochemical impedance spectroscopy characterization *J. Microelectromech. Syst.* **21** 1197–208
- [14] Gensler H, Sheybani R, Li P-Y, Mann R L and Meng E 2012 An implantable MEMS micropump system for drug delivery in small animals *Biomed. Microdevices* **14** 483–96
- [15] Shademani A, Zhang H, Jackson J K and Chiao M 2016 Active regulation of on-demand drug delivery by magnetically triggerable microspouters *Adv. Funct. Mater.* **27** 1604558
- [16] Shi J, Zhang H, Jackson J, Shademani A, Chiao M and Robust A 2016 Refillable magnetic sponge capsule for remotely triggered drug release *J. Mater. Chem. B* **4** 7415–22
- [17] Atik A C, Özkan M D, Özgür E, KÜlah H and Yıldırım E 2020 Modeling and fabrication of electrostatically actuated diaphragms for on-chip valving of MEMS-compatible microfluidic systems *J. Micromech. Microeng.* **30** 115001
- [18] Cazorla P H, Fuchs O, Cochet M, Maubert S, le Rhun G, Fouillet Y and Defay E 2016 A low voltage silicon micro-pump based on piezoelectric thin films *Sensors Actuators A* **250** 35–9
- [19] Yi Y, Huang R and Li C 2018 Flexible substrate-based thermo-responsive valve applied in electromagnetically powered drug delivery system *J. Mater. Sci.* **54** 3392–402
- [20] Shay T, Dickey M D and Velev O D 2017 Hydrogel-enabled osmotic pumping for microfluidics: towards wearable human-device interfaces *Lab Chip* **17** 710–6
- [21] Yi Y, Zaher A, Yassine O, Kosel J and Foulds I G 2015 A remotely operated drug delivery system with an electrolytic pump and a thermo-responsive valve *Biomicrofluidics* **9** 052608
- [22] Yang Y, Pan H, Xie G, Jiang Y, Chen C, Su Y and Tai H 2020 Flexible piezoelectric pressure sensor based on polydopamine-modified BaTiO<sub>3</sub>/PVDF composite film for human motion monitoring *Sensors Actuators A* **301** 111789
- [23] Kim H, Torres F, Wu Y, Villagran D, Lin Y and Tseng T L B 2017 Integrated 3D printing and corona poling process of PVDF piezoelectric films for pressure sensor application *Smart Mater. Struct.* **26** 085027
- [24] Wang J, Jiu J, Nogi M, Sugahara T, Nagao S, Koga H, He P and Sugauma K 2015 A highly sensitive and flexible pressure sensor with electrodes and elastomeric interlayer containing silver nanowires *Nanoscale* **7** 2926–32
- [25] Chen Y-M, He S-M, Huang C-H, Huang C-C, Shih W-P, Chu C-L, Kong J, Li J and Su C-Y 2016 Ultra-large suspended graphene as a highly elastic membrane for capacitive pressure sensors *Nanoscale* **8** 3555–64

- [26] Luo N, Dai W, Li C, Zhou Z, Lu L, Poon C C Y, Chen S-C, Zhang Y and Zhao N 2015 Flexible piezoresistive sensor patch enabling ultralow power cuffless blood pressure measurement *Adv. Funct. Mater.* **26** 1178–87
- [27] Yi Y, Samara A and Wang B 2020 A new approach for an ultra-thin piezoresistive sensor based on solidified carbon ink film *J. Mater. Sci.* **56** 607–14
- [28] Park S-J, Kim J, Chu M and Khine M 2017 Flexible piezoresistive pressure sensor using wrinkled carbon nanotube thin films for human physiological signals *Adv. Mater. Technol.* **3** 1700158
- [29] Zhao X, Hua Q, Yu R, Zhang Y and Pan C 2015 Flexible, stretchable and wearable multifunctional sensor array as artificial electronic skin for static and dynamic strain mapping *Electron. Mater.* **1** 1500142
- [30] Yamamoto Y, Harada S, Yamamoto D, Honda W, Arie T, Akita S and Takei K 2016 Printed multifunctional flexible device with an integrated motion sensor for health care monitoring *Sci. Adv.* **2** e1601473
- [31] Wang X, Gu Y, Xiong Z, Cui Z and Zhang T 2013 Silk-molded flexible, ultrasensitive, and highly stable electronic skin for monitoring human physiological signals *Adv. Mater.* **26** 1336–42
- [32] Wang C, Hwang D, Yu Z, Takei K, Park J, Chen T, Ma B and Javey A 2013 User-interactive electronic skin for instantaneous pressure visualization *Nat. Mater.* **12** 899–904
- [33] Chen X, Shao J, An N, Li X, Tian H, Xu C and Ding Y 2015 Self-powered flexible pressure sensors with vertically well-aligned piezoelectric nanowire arrays for monitoring vital signs *J. Mater. Chem. C* **3** 11806–14
- [34] Trung T Q and Lee N-E 2016 Flexible and stretchable physical sensor integrated platforms for wearable human-activity monitoring and personal healthcare *Adv. Mater.* **28** 4338–72
- [35] Wang Z et al 2016 High sensitivity, wearable, piezoresistive pressure sensors based on irregular microhump structures and its applications in body motion sensing *Small* **12** 3827–36
- [36] Kong J-H, Jang N-S, Kim S-H and Kim J-M 2014 Simple and rapid micropatterning of conductive carbon composites and its application to elastic strain sensors *Carbon* **77** 199–207
- [37] Yi Y, Wang B and Bermak A 2019 A low-cost strain gauge displacement sensor fabricated via shadow mask printing *Sensors* **19** 4713
- [38] Ali S, Khan S and Bermak A 2019 Inkjet-printed human body temperature sensor for wearable electronics *IEEE Access* **7** 163981–7
- [39] Wang L and Cheng L 2014 Piezoresistive effect of a carbon nanotube silicone-matrix composite *Carbon* **71** 319–31
- [40] Yi Y, Buttner U, Carreno A A A, Conchouso D and Foulds I G 2015 A pulsed-mode electrolytic drug delivery device *J. Micromech. Microeng.* **25** 105011
- [41] Pirmoradi F, Jackson J, Burt H and Chiao M 2011 On-demand controlled release of docetaxel from a battery-less MEMS drug delivery device *Lab Chip* **11** 2744
- [42] Liu M, Sun J, Sun Y, Bock C and Chen Q 2009 Thickness-dependent mechanical properties of polydimethylsiloxane membranes *J. Micromech. Microeng.* **19** 035028
- [43] Yi Y, Buttner U, Fan Y and Foulds I 2014 Design and optimization of a 3-coil resonance-based wireless power transfer system for biomedical implants *Int. J. Circuit Theory Appl.* **43** 1379–90
- [44] RamRakhyani A, Mirabbasi S and Chiao M 2011 Design and optimization of resonance-based efficient wireless power delivery systems for biomedical implants *IEEE Trans. Biomed. Circuits Syst.* **5** 48–63